


**Spin inhomogeneities at the interface and inverted hysteresis loop in  $\text{La}_{0.7}\text{Sr}_{0.3}\text{MnO}_3/\text{SrTiO}_3$** 

Pramod Ghising, B. Samantaray, and Z. Hossain\*

*Department of Physics, Indian Institute of Technology, Kanpur 208016, India* (Received 19 September 2019; revised manuscript received 30 November 2019; published 14 January 2020)

An inverted hysteresis loop (IHL) exhibits negative coercivity and remanence, and has been ascribed to various mechanisms ranging from exchange coupling to competing anisotropies and even experimental artifacts. Here, we investigate the IHL behavior of monolithic  $\text{La}_{0.7}\text{Sr}_{0.3}\text{MnO}_3$  (LSMO) film using magnetization and ferromagnetic resonance (FMR) studies at 300 K. FMR measurements reveal the presence of fourfold ( $K_4 = 5.7 \times 10^2 \text{ erg cm}^{-3}$ ), uniaxial ( $K_u = 1.9 \times 10^2 \text{ erg cm}^{-3}$ ), and exchange ( $K_{A/F} = -1.15 \times 10^3 \text{ erg cm}^{-3}$ ) anisotropy. It is known that the competition of fourfold and uniaxial anisotropy can lead to an IHL. Furthermore, magnetic measurements exhibit positive exchange bias (EB), which could also lead to an IHL. The appearance of positive EB in monolithic LSMO film indicates the presence of secondary phases and an antiferromagnetic (AFM) coupling between the phases. We show unambiguously that the observed IHL is a result of interfacial exchange coupling in the LSMO film. Using FMR, we verify the AFM coupling at the interface and, in conjunction with the results of an earlier report, we develop an intuitive picture for the spin arrangement at the interface. Our study reveals a complex interface physics in LSMO/ $\text{SrTiO}_3$  (STO), whose understanding may generate new pathways for the development of novel functionalities in LSMO.

DOI: [10.1103/PhysRevB.101.024408](https://doi.org/10.1103/PhysRevB.101.024408)**I. INTRODUCTION**

Complex oxide films with their myriad of exotic phenomena present a fertile research ground for the scientific community. Thin films, unlike their bulk counterpart, come with an additional advantage: the freedom to create an interface between different compounds. The interface often triggers the birth of novel physics, which otherwise is absent in the bulk form, e.g., two-dimensional electron gas at polar-nonpolar oxides [1,2], interfacial superconductivity [3], interfacial magnetism [4,5], and exchange bias [6–8]. The interface stands unrivaled in its complexity as well as opportunities to integrate different functionalities for better and efficient devices.

The exchange bias (EB) effect is one of the most widely studied interface phenomena. It has its origin in the exchange coupling of magnetic moments at the interface between a ferromagnet and an antiferromagnet. Beginning with the work of Meiklejohn *et al.* [9,10], it has come a long way and has paved the way for many novel devices [11–13]. Another very intriguing interface phenomena is the inverted hysteresis loop (IHL), which exhibits negative coercivity and remanence values [14–17]. This unconventional hysteresis behavior in magnetic heterostructures has been attributed to interfacial exchange coupling [14–17] and competing anisotropies [18,19]. Even more interesting is the observation of the IHL in monolithic films [20–22].

In this work, we present our results on the IHL behavior in  $\text{La}_{0.7}\text{Sr}_{0.3}\text{MnO}_3$  (LSMO) film. The film is deposited on  $\text{TiO}_2$  terminated  $\text{SrTiO}_3$  substrate. So far, the IHL in monolithic films has been attributed to antiferromagnetic (AFM) exchange coupling between different magnetic phases [21,22].

However, to arrive at a definitive conclusion, one also needs to consider the possibility of competing anisotropies as the source of an IHL in the monolithic film. Here, we employ the ferromagnetic resonance (FMR) technique to investigate the role of magnetic anisotropies in the observed IHL. Also, the results of our magnetization and FMR measurements reveal a spiral arrangement of magnetic moments at the interface.

**II. EXPERIMENTAL DETAILS**

LSMO film with a thickness of 150 Å was grown on a  $\text{SrTiO}_3$  (001) substrate. Pulsed laser deposition, with a KrF excimer laser (Lambda Physik COMPexPro,  $\lambda = 248 \text{ nm}$ ) was used for film fabrication.  $\text{SrTiO}_3$  (STO) substrate was etched with a  $\text{NH}_4\text{HF}$  solution to obtain a  $\text{TiO}_2$  terminated surface. A substrate temperature of 730 °C and an oxygen background pressure of 0.2 mbar were maintained during film deposition. A polycrystalline target of LSMO was prepared using the solid-state reaction method. The crystalline structure of the film was studied using an x-ray diffractometer (PANalytical X'Pert PRO,  $\lambda = 1.5405 \text{ Å}$ ). Magnetic and transport measurements were performed in a Physical Property Measurement System (PPMS-Quantum Design). The FMR measurements were carried out using a Bruker EMX electron paramagnetic resonance (EPR) spectrometer, with the sample mounted inside a resonant cavity of resonance frequency  $\approx 9.6 \text{ GHz}$ .

**III. RESULTS AND DISCUSSION**

In Fig. 1, we show the results of structural characterization, electrical, and magnetization measurement on LSMO/STO film. The x-ray diffraction (XRD) plot in Fig. 1(a) shows only

\*zakir@iitk.ac.in

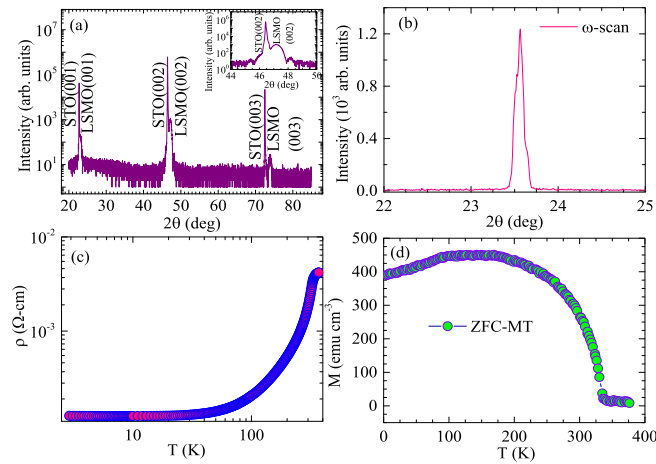


FIG. 1. (a) XRD plot showing the film and the substrate reflections. The epitaxial nature of the film is confirmed by the presence of only (00 $l$ )-oriented film peaks. Inset: the (002) film and substrate reflection. (b)  $\omega$  scan around the (002) film peak. The low value of the FWHM ( $0.11^\circ$ ) indicates good crystalline structure of the film. (c) Temperature variation of resistivity of the LSMO film. (d) ZFC- $M(T)$  data acquired during the heating cycle. A field of 100 Oe was applied during the data acquisition.

(00 $l$ )-oriented film peaks, which confirms epitaxial growth of the LSMO film. The inset in Fig. 1(a) shows (002) XRD peaks of the film and the substrate. Also, the very low value ( $0.11^\circ$ ) of the full width at half maximum (FWHM) obtained from the  $\omega$  scan [see Fig. 1(b)] indicates a very good crystalline structure of the film. The temperature dependence of resistivity [ $\rho(T)$ ] for LSMO/STO is shown in Fig. 1(c). It exhibits metallic behavior in the entire temperature range of the measurement. Figure 1(d) displays the temperature variation of magnetization  $M(T)$  in the zero-field-cooled (ZFC) protocol. The sample was cooled down to 7 K in zero applied field. The  $M(T)$  data were taken during the heating cycle, with an applied field of 100 Oe. The ferromagnetic (FM) transition temperature  $T_C$  was estimated to be 330 K.

Magnetic hysteresis  $M(H)$  measurements were carried out at 300 K, with field applied along the [100] direction. In order to remove the remnant field in the sample, the magnet was demagnetized in oscillation mode from 5000 Oe at 380 K (much above  $T_C$ ).  $M(H)$  measurement was also performed on a standard Pd sample to estimate the remnant field due to the superconducting magnet coils, which is very low ( $\approx 2$  Oe). In Fig. 2(a), we show the enlarged central portion of the  $M(H)$  loop. The blue and black arrows denote paths followed by the field sweep. The inset in Fig. 2(a) shows  $M(H)$  data in the entire field range of  $\pm 5000$  Oe. Low coercivity,  $H_c \approx \pm 11$  Oe, is obtained, which is consistent with earlier reports [22]. A very notable result is the partial inversion of the hysteresis loop shown in Fig. 2(a). Earlier reports have attributed partial and complete IHL to the presence of EB effects [20–22], competing anisotropies in the system [18,19], etc. In our sample, a shift in the  $M(H)$  loop was also observed at low scan fields [shown in Fig. 2(b)], typical of the EB effect. For EB measurements, the sample was cooled down from 380 K (much above  $T_C$ ) to 300 K in an in-plane field

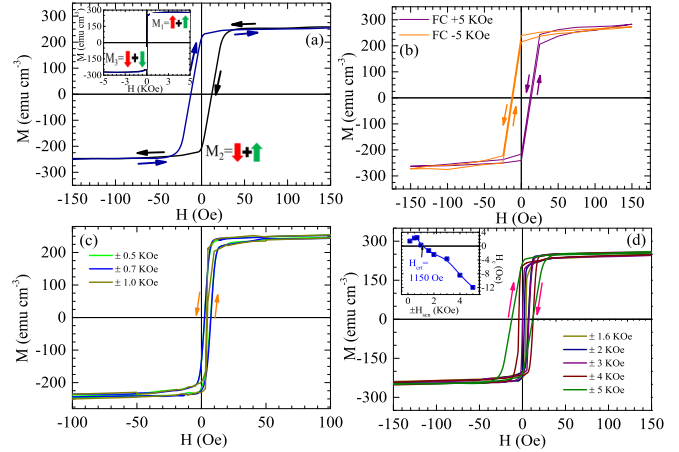


FIG. 2. Measurement of hysteresis loop at 300 K. (a) Hysteresis loop measured at 300 K with field applied along [100]. The black and the blue arrows denote the direction of the field sweep. The central portion of the loop has been enlarged to show the IHL behavior. The inset in (a) shows the full loop measured in a field range of  $\pm 5000$  Oe. The bold red and green arrows represent the magnetization direction of the stoichiometric soft and the Sr-rich hard layer, respectively. (b) Positive EB loops measured under low scan field range of  $\pm 150$  Oe after field cooling of  $\pm 5000$  Oe from 380 K. (c), (d) Hysteresis loops measured under different scan field ranges. At low scan fields, IHL is absent as shown in (c), while for higher scan fields in (d), the loop is inverted. The inset in (d) displays loop coercivity as a function of scan field ( $H_{scn}$ ). From the upper inset, it is seen that the loop inversion occurs at  $H_{crit} \approx \pm 1150$  Oe.

of  $\pm 5000$  Oe (higher than the saturation fields). The  $M(H)$  loops were measured in the field range of  $\pm 150$  Oe. We observed positive exchange bias in our sample, i.e., loop shift in the same direction as the cooling field, as opposed to conventional exchange bias where the loop shift is in the opposite direction of the cooling field. Furthermore, inversion of the hysteresis loop disappears at low scan fields, as can be seen in Fig. 2(b). It was also observed that the exchange biased loops for positive and negative cooling fields [Fig. 2(b)] coincide with the descending and ascending branch of the IHL in Fig. 2(a), respectively. Additionally,  $M(H)$  loops measured at different scan field ranges  $H_{scn}$  reveal a critical field at which the inversion of the  $M(H)$  loop commences. We show the results for hysteresis loops with different scan fields in Figs. 2(c) and 2(d). Figure 2(c) displays the hysteresis loops at low scan fields where the loops are not inverted, while at higher scan fields, the IHL is observed, as shown in Fig. 2(d). The upper inset in Fig. 2(d) shows  $H_c$  as a function of  $H_{scn}$ ; it reveals a critical field,  $H_{crit} \approx \pm 1150$  Oe, above which the IHL is observed.

A prerequisite for EB is the presence of FM-AFM or hard/soft FM-FM interface that generates a unidirectional anisotropy in the system. Since our sample consists of a monolithic LSMO film, the observation of EB is likely due to the presence of secondary phases. Also, the observed positive exchange bias indicates an AFM coupling between the different phases. In an earlier work, Saghayezhian *et al.* reported the formation of a very thin layer of Sr-rich phases ( $\text{La}_{0.40}\text{Sr}_{0.60}\text{MnO}_3$  and  $\text{La}_{0.55}\text{Sr}_{0.45}\text{MnO}_3$ ) at the interface that

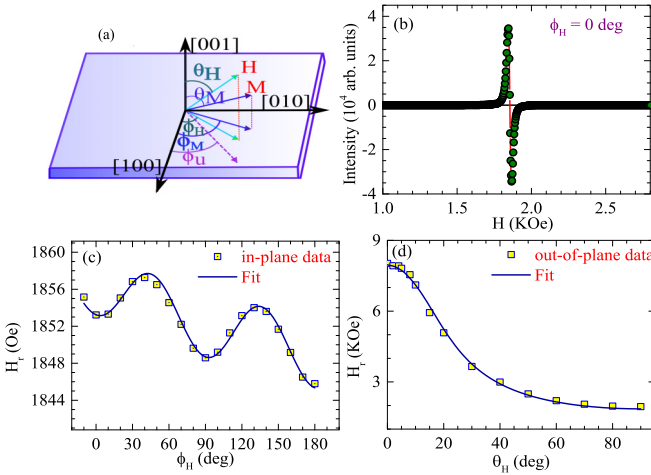


FIG. 3. (a) Schematic of the magnetization, applied field, and anisotropy direction with respect to the sample plane. (b) In-plane FMR spectrum at 300 K with field applied along [100]. (c) Resonance field as a function of in-plane angle  $\phi_H$ . The solid line represents a fit to the experimental data using Eq. (2). (d) Resonance field as a function of out-of-plane angle  $\theta_H$ . The solid line shows a fit to the experimental data.

couple antiferromagnetically to the rest of the stoichiometric LSMO layers [22]. The Sr-rich phase reportedly extends to only two layers from the STO surface [22]. The first Sr-rich layer  $\text{La}_{0.40}\text{Sr}_{0.60}\text{MnO}_3$  is antiferromagnetically coupled to the stoichiometric bulk layer, whereas the second Sr-rich layer ( $\text{La}_{0.55}\text{Sr}_{0.45}\text{MnO}_3$ ) acts as a transition layer with 50% of its moments coupled ferromagnetically to both the first Sr-rich layer and the rest of the stoichiometric layers [22]. Therefore, the LSMO film can be thought of as a stoichiometric soft magnetic layer antiferromagnetically coupled to a Sr-rich hard magnetic layer at the interface. Saghayezhian *et al.* [22] attributed the IHL to AFM coupling at the interface. However, contribution from other sources, mainly the presence of competing anisotropies in the film, also has to be considered in order to arrive at a definitive conclusion.

To investigate the different magnetic anisotropies in our sample, we resort to FMR measurements. In Fig. 3(a), a representative sketch of the magnetization  $M$ , applied field  $H$ , and anisotropy directions with respect to the sample plane is shown. Figure 3(b) displays the in-plane FMR spectrum for LSMO film with magnetic field applied along the [100] direction. The variation of resonance field  $H_r$  as a function of in-plane angle  $\phi_H$  and out-of-plane angle  $\theta_H$  is shown in Figs. 3(c) and 3(d), respectively. The in-plane  $H_r$  variations exhibit a strong fourfold anisotropy, with the easy axis along the [100] direction. For analysis of the FMR data, the energy density of the LSMO film is given by [23–25]

$$\begin{aligned}
 E = & -M_s H [\sin \theta_M \sin \theta_H \cos(\phi_M - \phi_H) + \cos \theta_M \cos \theta_H] \\
 & - 2\pi M_s^2 \sin^2 \theta_M - K_u \sin^2 \theta_M \\
 & \times \cos^2(\phi_M - \phi_u) + K_p \sin^2 \theta_M \\
 & - \frac{K_4}{8} [7 + \cos 4(\phi_M - \phi_4)] \sin^4 \theta_M \\
 & - K_{A/F} \sin \theta_M \cos \phi_M,
 \end{aligned} \quad (1)$$

where the energy terms in Eq. (1), in order of their appearance, are the Zeeman energy, dipolar energy, in-plane uniaxial anisotropy energy, perpendicular anisotropy energy, fourfold magnetocrystalline energy, and exchange anisotropy energy.  $K_u$ ,  $K_p$ ,  $K_4$ , and  $K_{A/F}$  represent the in-plane uniaxial anisotropy, perpendicular anisotropy, fourfold magnetocrystalline anisotropy, and exchange anisotropy, respectively. The resonance condition formulated by Smit and Beljers is given by the following expression [23]:

$$\frac{2\pi f_r}{\gamma} = \frac{1}{M_s \sin \theta_M} \sqrt{\frac{\partial^2 E}{\partial \theta_M^2} \frac{\partial^2 E}{\partial \phi_M^2} - \frac{\partial^2 E}{\partial \theta_M \partial \phi_M}}, \quad (2)$$

where  $f_r$  is the resonance frequency,  $M_s$  is the saturation magnetization,  $\gamma = g\mu_B/\hbar$  is the gyromagnetic ratio,  $g$  is the  $g$  factor, and  $\mu_B$  is the Bohr magneton.

The equilibrium angles of magnetization  $\phi_M$  and  $\theta_M$  are numerically determined for each values of  $\phi_H$  and  $\theta_H$  by minimizing the total free-energy density in Eq. (1),

$$\frac{\partial E}{\partial \phi_M} = \frac{\partial E}{\partial \theta_M} = 0. \quad (3)$$

The expression for  $H_r$  as a function of  $\phi_H$  and  $\theta_H$  is obtained from Eqs. (2) and (3), which is then used to fit the experimental data as shown in Figs. 3(c) and 3(d), respectively. From the fitting procedure, we obtain  $g = 2.02$ , which is very similar to the values reported earlier for LSMO/STO(001) [26]. The anisotropy parameters obtained from the fitting procedure are  $K_u = 1.9 \times 10^2$ ,  $K_4 = 5.7 \times 10^2$ ,  $K_p = -1.35 \times 10^5$ , and  $K_{A/F} = -1.15 \times 10^3$  erg cm $^{-3}$ . As  $K_4 > K_u$ , fourfold anisotropy dominates the in-plane angular  $H_r$  variations, which agrees with our experimental observations [see Fig. 3(c)]. A very interesting parameter is  $K_{A/F}$ , which arises as a result of exchange coupling in the system. To achieve a very good fit of the experimental data, it is imperative to consider the contribution of the exchange coupling and the uniaxial anisotropy term. From the fitting of the in-plane FMR data in Fig. 3(c), we find that the easy axis (EA) of  $K_4$  lie along in-plane  $\langle 100 \rangle$ , while that of  $K_u$  lies along [110] and  $[-1 - 10]$ . Also, from the  $H_r(\phi_H)$  plot in Fig. 3(c), we obtain an EB field [ $H_r(0) - H_r(180)$ ] of  $\approx 7.4$  Oe, which is comparable to that obtained from  $M(H)$  measurements ( $\approx 11$  Oe). Thus, the FMR measurements are in agreement with the  $M(H)$  data, which exhibit exchange bias. Furthermore, the sign of  $K_{A/F}$  (negative) suggests an AFM alignment of the moments at the interface, which is again consistent with the positive EB observed in the  $M(H)$  measurements.

FWHM or the linewidth  $\Delta H$  of the FMR spectrum as a function of  $\theta_H$  is shown in Fig. 4(a).  $\Delta H$  reflects the spin dynamics in a magnetic system and is representative of spin-relaxation mechanisms in the system. There are two factors contributing to the damping mechanism: intrinsic and extrinsic [27,28],

$$\Delta H = \frac{1}{\sqrt{3}} \Delta H_\alpha + \frac{1}{\sqrt{3}} \Delta H_{ex}. \quad (4)$$

The first term in Eq. (4) is the intrinsic contribution, where

$$\Delta H_\alpha = \frac{\alpha}{M_s} \left[ \frac{\partial^2 E}{\partial \theta_M^2} + \frac{1}{\sin^2 \theta_M} \frac{\partial^2 E}{\partial \phi_M^2} \right] \left| \frac{\partial (\frac{2\pi f_r}{\gamma})}{\partial H_r} \right|^{-1} \quad (5)$$

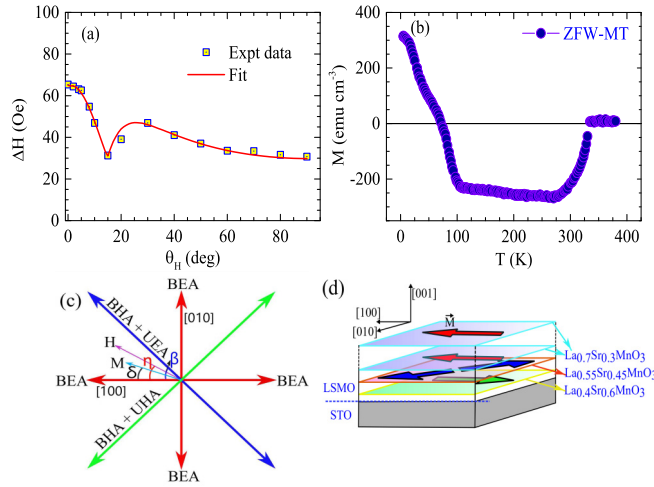


FIG. 4. (a) FMR linewidth variation with out-of-plane field angle  $\theta_H$ . Equation (4) is used to fit the experimental data (solid blue line). (b) Remanent magnetization as a function of temperature. The sample was cooled in a field of 1500 Oe, applied along  $[100]$ . The data were taken during the ZFW cycle. (c) Anisotropy directions in the LSMO film obtained from FMR measurements. (d) Schematic of the LSMO film showing the first and second Sr-rich layer at the interface. From the third layer onward, the film recovers its bulk stoichiometry. The bold arrows represent the magnetization direction in the different layers. The arrangement of the layer magnetization was conceived from the results of our FMR and  $M(H)$  measurements, and the result displayed in Fig. 5 of Ref. [22].

is the Gilbert term with  $\alpha$  as the damping parameter. The extrinsic term is attributed to inhomogeneity at the interface and is written as

$$\Delta H_{ex} = \left| \frac{dH_r}{d(4\pi M_{\text{eff}})} \right| \Delta(4\pi M_{\text{eff}}) + \left| \frac{dH_r}{d\theta_H} \right| \Delta\theta_H. \quad (6)$$

The first term in Eq. (6) is ascribed to the inhomogeneous variation of effective magnetization ( $4\pi M_{\text{eff}} = 4\pi M_s - \frac{2K_p}{M_s}$ ) at the interface. And the second term is related to the dispersion of the anisotropy axis on account of structural inhomogeneities at the interface.

In Fig. 4(a), we show the results of fitting the experimental data of  $\Delta H$  vs  $\theta_H$  with Eq. (4). From the results of the fitting, we extract the values for  $\alpha$  ( $=1.9 \times 10^{-3}$ ),  $\Delta 4\pi M_{\text{eff}}$  ( $=115$  Oe), and  $\Delta\theta_H$  ( $\approx 0.02^\circ$ ). The value of  $\alpha$  is comparable to that reported in Ref. [23]. The low value of  $\alpha$  indicates good sample homogeneity. Also, it is seen that the contribution to  $\Delta H$  due to structural inhomogeneities is negligible (since  $\Delta\theta_H \approx 0.02^\circ$  is very small).

The FMR experiments yield two very interesting results. First, the presence of both fourfold and uniaxial anisotropy and, second, the inhomogeneity of  $4\pi M_{\text{eff}}$  at the interface. The presence of two competing anisotropies have also been known to give rise to an IHL in thin films [18,19]. Thus, in our sample, we have two possible mechanisms for the origin of an IHL: competing anisotropies and interfacial exchange coupling. In the earlier models [18,19] used to explain the IHL due to competing anisotropies, the hysteresis loop was measured with field applied along the hard axis. Therefore, at high values of  $H$  [in the saturation region of the  $M(H)$  loop],

$M$  is aligned along the hard axis. As  $H$  is lowered [descending branch of the  $M(H)$  loop],  $M$  continuously rotates towards the easy axes (away from the direction of  $H$ ), owing to the presence of competing anisotropies (see Fig. 7 of Ref. [18]). Consequently, if at remanence the angle between  $M$  and  $H$  is  $>90^\circ$ , an IHL is observed. Otherwise, the loop is not inverted [18,19]. In the LSMO film, the four easy axes (BEA) of the fourfold anisotropy lie along the in-plane  $\langle 100 \rangle$ , while the four hard axes (BHA) lie along the in-plane  $\langle 110 \rangle$ . Furthermore, the uniaxial anisotropy also has its easy axis (UEA) along the  $[110]$  direction. The anisotropy axes in the sample plane (obtained from FMR measurements) along with  $M$  and  $H$  are illustrated in Fig. 4(c), where  $\eta$  and  $\delta$  represent the directions of  $H$  and  $M$  with respect to BEA, respectively, and  $\beta$  is the angle between BEA and UEA. Along  $\langle 110 \rangle$ , there is a superposition of BHA and uniaxial anisotropy axes, as shown in Fig. 4(c). In the  $M(H)$  loop, Zeeman energy dominates at higher  $H$  values, while at low fields the anisotropy energy gradually overcomes the Zeeman energy. For the LSMO film, the  $M(H)$  measurement was carried out with  $\eta = 0^\circ$  ( $H$  along  $[100]$  BEA) and  $\beta = 45^\circ$ . The Zeeman energy aligns  $M$  along  $H$  (which coincides with BEA), while the competing anisotropies (at low fields) try to align  $M$  along one of its corresponding easy axes. From Fig. 4(c), it is evident that BEA is in a lower-energy state compared to UEA, i.e.,  $E_{100} < E_{110}$ ; so the sample anisotropy also favors the alignment of  $M$  along BEA. Therefore,  $M$  stays very close to BEA both at high and low  $H$ . As a consequence,  $M$  does not move significantly away from its initial position when the field is lowered, and hence the condition for the IHL, i.e.,  $\delta - \eta > 90^\circ$  at  $H = 0$  [18,19] is never met. Therefore, competing anisotropies should not give rise to the IHL in the LSMO film. Furthermore,  $K_4/K_u = 3$  suggests that the fourfold anisotropy is comparatively too strong and hence will not lead to the IHL in the LSMO film [18]. These results provide compelling evidence that EB (due to interfacial AFM exchange coupling) is responsible for the IHL rather than the competing anisotropies in the LSMO film.

An explanation for the observed IHL is given as follows.  $H_{\text{crit}}$  obtained from the upper inset of Fig. 2(d) is a measure of the anisotropy field of the hard magnetic layer at the interface. This is because only above  $H_{\text{crit}}$  can the external field align the hard layer moments. For  $H_{\text{scn}} < H_{\text{crit}}$ , only the soft magnetic layer switches its magnetization with the applied field [ $M_2$  region in Fig. 2(a)], and therefore the hysteresis loop is not inverted; however, positive EB is observed as the soft layer is antiferromagnetically coupled with the hard layer [lower inset of Fig. 2(d)]. For  $H_{\text{scn}} > H_{\text{crit}}$ , magnetization of both the hard and soft layers follows the applied field direction. This sets the stage for the appearance of an IHL. For  $H > H_{\text{crit}}$ , magnetization of both layers switches with the applied field [ $M_1$  and  $M_3$  region in the inset of Fig. 2(a)] and they are aligned along the field direction. As the field is lowered below  $H_{\text{crit}}$ , the soft magnetic layers start to follow the field direction and gradually reverse, while the hard layer remains aligned in its initial direction. Since the hard and soft layers favor AFM coupling, energy considerations also favor the reversal of the soft magnetic layer. This ensures that the soft layer reversal occurs at a lower energy [positive quadrant of the  $M(H)$  loop], which leads to negative remanence. Hence, the descending branch of the loop exhibits negative coercivity.

The same argument applies for the ascending branch of the  $M(H)$  loop.

The inhomogeneous  $4\pi M_{\text{eff}}$  is a direct consequence of the AFM exchange coupling at the interface. According to Saghayezhian *et al.* [22], the net magnetic moment of the first Sr-rich layer is aligned antiparallel with the stoichiometric bulk layers, while the net magnetization of the second Sr-rich layer is  $\approx 0$ . We propose that the second Sr-rich layer gives rise to the observed uniaxial anisotropy in our sample, with moments aligned along the [110] and  $[-1 - 10]$  easy direction (so that the net magnetization is zero), whereas the dominant fourfold anisotropy is due to the bulk stoichiometric layers. Based on the results of the FMR experiment, an intuitive picture of the magnetic moment alignment in the interface region is shown in Fig. 4(d). The AFM coupling leads to a Bloch domain-wall-like spiral arrangement of moments across the interfacial Sr-rich and stoichiometric layers, which presents as the inhomogeneous distribution of  $4\pi M_{\text{eff}}$  in the FMR experiment. Also, the Bloch domain-wall-like arrangement of moments is feasible as it lowers the exchange interaction energy between the neighboring layers. The spiral alignment of the magnetic moments at the interface imparts an exchange springlike [29] characteristic to the LSMO film. This is apparent from the remanent magnetization measurement described in the following paragraph.

Figure 4(b) shows the remanent magnetization data for the LSMO film. The sample was cooled down to 7 K in the presence of a magnetic field ( $=1500$  Oe), applied along [100]. At 7 K, the field was switched off and data were acquired during the zero-field-warming (ZFW) cycle. After field cooling at 7 K, magnetization of both the hard and soft layers is aligned in the same direction. This state is energetically unfavorable as the interfacial Sr-rich and stoichiometric bulk layers favor AFM exchange coupling, which is evident from the observed positive EB in Fig. 2(b). So on removing the field, magnetic moments of the soft layer gradually start to rotate in the opposite direction. Spontaneous magnetic reversal (SMR) is observed at  $\approx 71$  K. From Fig. 2(a), a rough estimate of the hard layer magnetization  $M_{\text{hard}}$  can be made as follows:  $M_{\text{hard}} = (M_1 + M_2)/2 \approx 3 \mu_B/\text{f.u.}$  Now we can estimate the anisotropy of the hard layer,  $K_{\text{hard}} = H_{\text{crit}} M_{\text{hard}} \approx 5 \times 10^5 \text{ erg cm}^{-3}$ . Based on the anisotropy energy considerations of the different layers, an argument for the spontaneous reversal can be made as follows. During ZFW, the uniaxial anisotropy will align the transition layer (Sr-rich second layer) moments along its easy axis ([110] and  $[-1 - 10]$ ), while hard layer (Sr-rich first layer) moments remain aligned along the initial field direction. As  $K_4 < K_{\text{hard}}$ , it is much easier to rotate the moments of the soft magnetic layer. Consequently, the transition layer moments now generate a torque on the third (stoichiometric bulk) layer moments. This torque rotates

the moments of the third layer by  $180^\circ$  to lie antiparallel to the first layer. Since the bulk layers favor ferromagnetic exchange coupling, the moments in the rest of the soft layers gradually rotate parallel to that of the stoichiometric third layer. This results in a complete reversal of the soft layer moments with increasing temperature and leads to SMR.

#### IV. CONCLUSIONS

In summary, we have observed an IHL in LSMO/STO films at 300 K. From  $M(H)$  measurements carried out at different scan fields, we obtain a critical field,  $H_{\text{crit}} \approx 1150$  Oe, below which the inversion of the hysteresis loop disappears. Furthermore, positive EB is observed in the LSMO sample, which points to the presence of an AFM coupled secondary phase at the interface. In order to have a better understanding of the IHL, we have studied the magnetic anisotropies pertinent to our system using the FMR technique. Fitting the in-plane  $H_r(\phi_H)$  data reveals the presence of both fourfold and uniaxial anisotropy with EA along (100) and [110], respectively. This result points to two sources of the IHL in the LSMO film: interfacial exchange coupling and competing anisotropies. Our results indicate that the observed IHL is due to interfacial exchange coupling, and not due to the competing anisotropies. EB is ascribed to the presence of a Sr-rich layer at the interface, antiferromagnetically coupled to the stoichiometric bulk layers. Furthermore, fitting the experimental data for the out-of-plane FMR spectrum  $\Delta H(\theta_H)$  reveals an inhomogeneous distribution of magnetization at the interface. The magnetic inhomogeneity at the interface stems from a spiral arrangement of the magnetic moments at the interface. The spiral alignment lends an exchange springlike characteristic to the LSMO film. Exchange springlike behavior of the film is apparent in the remanent magnetization measurement, where the soft layer moments start to reverse due to a torque generated by the transition layer after the field is removed. This reversal continues until all the moments are reversed, leading to a negative magnetization value. Our work explores a very intriguing aspect of the interface phenomena, wherein an EB is observed in single monolithic ferromagnetic films at room temperature. Our experiments uncover the physics behind the IHL phenomena in monolithic thin films. The complex arrangement of spins along with EB in single-component ferromagnetic films may be useful in developing new spintronics applications.

#### ACKNOWLEDGMENTS

The authors would like to thank R. C. Budhani for the valuable discussion and Veena Singh for her help with the FMR measurements. Financial support from IIT Kanpur is gratefully acknowledged.

- [1] A. Ohtomo, D. A. Muller, J. L. Grazul, and H. Y. Hwang, *Nature (London)* **419**, 378 (2002).
- [2] A. Ohtomo and H. Y. Hwang, *Nature (London)* **427**, 423 (2004).
- [3] N. Reyren, S. Thiel, A. D. Caviglia, L. F. Kourkoutis, G. Hammerl, C. Richter, C. W. Schneider, T. Kopp, A.-S. Rüetschi,

D. Jaccard, M. Gabay, D. A. Muller, J.-M. Triscone, and J. Mannhart, *Science* **317**, 1196 (2007).

- [4] K. S. Takahashi, M. Kawasaki, and Y. Tokura, *Appl. Phys. Lett.* **79**, 1324 (2001).
- [5] M. Keunecke, F. Lyzwa, D. Schwarzbach, V. Roddatis, N. Gauquelin, K. Müller-Caspary, J. Verbeeck, S. J. Callori,

- F. Klose, M. Jungbauer, and V. Moshnyaga, *Adv. Funct. Mater.* **29**, 1808270 (2019).
- [6] M. Gibert, P. Zubko, R. Scherwitzl, J. Íñiguez, and J.-M. Triscone, *Nat. Mater.* **11**, 195 (2012).
- [7] X. Ke, M. S. Rzechowski, L. J. Belenky, and C. B. Eom, *Appl. Phys. Lett.* **84**, 5458 (2004).
- [8] J. C. Rojas Sánchez, B. Nelson-Cheeseman, M. Granada, E. Arenholz, and L. B. Steren, *Phys. Rev. B* **85**, 094427 (2012).
- [9] W. H. Meiklejohn and C. P. Bean, *Phys. Rev.* **102**, 1413 (1956).
- [10] W. H. Meiklejohn and C. P. Bean, *Phys. Rev.* **105**, 904 (1957).
- [11] J. Nogués and I. K. Schuller, *J. Magn. Magn. Mater.* **192**, 203 (1999).
- [12] D. Lacour, H. Jaffrès, F. Nguyen Van Dau, F. Petroff, A. Vaurès, and J. Humbert, *J. Appl. Phys.* **91**, 4655 (2002).
- [13] Ching Tsang, R. E. Fontana, Tsann Lin, D. E. Heim, V. S. Speriosu, B. A. Gurney, and M. L. Williams, *IEEE Trans. Magn.* **30**, 3801 (1994).
- [14] K. Takanashi, H. Kurokawa, and H. Fujimori, *Appl. Phys. Lett.* **63**, 1585 (1993).
- [15] M. J. O'Shea and A. Al-Sharif, *J. Appl. Phys.* **75**, 6673 (1994).
- [16] Y. Z. Wu, G. S. Dong, and X. F. Jin, *Phys. Rev. B* **64**, 214406 (2001).
- [17] M. Ziese, I. Vrejoiu, and D. Hesse, *Appl. Phys. Lett.* **97**, 052504 (2010).
- [18] S. M. Valvidares, L. M. Álvarez-Prado, J. I. Martín, and J. M. Alameda, *Phys. Rev. B* **64**, 134423 (2001).
- [19] Y. Jae Nam and S. H. Lim, *Appl. Phys. Lett.* **99**, 092503 (2011).
- [20] K. G. West, D. N. H. Nam, J. W. Lu, N. D. Bassim, Y. N. Picard, R. M. Stroud, and S. A. Wolf, *J. Appl. Phys.* **107**, 113915 (2010).
- [21] T. Maity, D. Kepaptsoglou, M. Schmidt, Q. Ramasse, and S. Roy, *Phys. Rev. B* **95**, 100401(R) (2017).
- [22] M. Saghayezhian, S. Kouser, Z. Wang, H. Guo, R. Jin, J. Zhang, Y. Zhu, S. T. Pantelides, and E. W. Plummer, *Proc. Natl. Acad. Sci.* **116**, 10309 (2019).
- [23] H. K. Lee, I. Barsukov, A. G. Swartz, B. Kim, L. Yang, H. Y. Hwang, and I. N. Krivorotov, *AIP Adv.* **6**, 055212 (2016).
- [24] M. J. Pechan, D. Bennett, N. Teng, C. Leighton, J. Nogués, and I. K. Schuller, *Phys. Rev. B* **65**, 064410 (2002).
- [25] M. Belmeguenai, S. Mercone, C. Adamo, L. Méchin, C. Fur, P. Monod, P. Moch, and D. G. Schlom, *Phys. Rev. B* **81**, 054410 (2010).
- [26] Åsmund Monsen, J. E. Boschker, F. Macià, J. W. Wells, P. Nordblad, A. D. Kent, R. Mathieu, T. Tybell, and E. Wahlström, *J. Magn. Magn. Mater.* **369**, 197 (2014).
- [27] S. Mizukami, Y. Ando, and T. Miyazaki, *Phys. Rev. B* **66**, 104413 (2002).
- [28] S. J. Yuan, L. Sun, H. Sang, J. Du, and S. M. Zhou, *Phys. Rev. B* **68**, 134443 (2003).
- [29] E. E. Fullerton, J. Jiang, and S. Bader, *J. Magn. Magn. Mater.* **200**, 392 (1999).